Multimodal piezoelectric energy harvesting on a thin plate integrated with SSHI circuit: an analytical and experimental study

OPEN ACCESS
IOP Publishing
Smart Materials and Structures
Smart Mater. Struct. **32** (2023) 095024 (12pp)
https://doi.org/10.1088/1361-665X/ace9a0

Multimodal piezoelectric energy harvesting on a thin plate integrated with SSHI circuit: an analytical and experimental study

Seyed Morteza Hoseyni[1], Mehmet Simsek[1], Amirreza Aghakhani[2], Elie Lefeuvre[3] and Ipek Basdogan[1,*]

[1] Mechanical Engineering Department, College of Engineering, Koc University, Istanbul 34450, Turkey
[2] School of Engineering, Newcastle University, Newcastle upon Tyne, United Kingdom
[3] Centre for Nanoscience and Nanotechnology, Université Paris-Saclay—CNRS, Palaiseau F-91120, France

E-mail: ibasdogan@ku.edu.tr

Received 8 April 2023, revised 18 June 2023
Accepted for publication 21 July 2023
Published 11 August 2023

Abstract

Multimodal piezoelectric energy harvesting can be achieved by integrating piezo-patch harvesters into plate-like structures available in marine, aerospace, and automotive applications. A synchronized switch harvesting on inductor (SSHI) interface as the harvesting circuit has been well studied for cantilever beams, considering the single vibration mode of the structure. However, integrating a two-dimensional electromechanical structure with a SSHI circuit for multimodal energy harvesting is missing in the literature. This paper evaluates the performance of the SSHI interface integrated with a piezoelectric energy harvester (PEH) on a plate-like host structure. The analytical solution is developed based on an equivalent impedance approach to predict the steady-state electrical response of the harvester as a closed-form solution. The experiments are conducted to validate the analytical solution for the system's first and second vibration modes. The experimental results reveal that integration of SSHI to a plate-like harvester introduces a multi-switching behavior rather than a standard single-switching behavior. Due to the multimodal vibrational characteristics of the plate, the circuit switch is triggered several times at each half period of the vibration, which increases the energy dissipation of the circuit and thus reduces the output voltage. On the other hand, single switching at each half period of the vibration happens for lower piezoelectric voltage levels. This is the desired behavior of the SSHI circuit where the analytical prediction matches with the experimental data. Finally, the energy harvesting performance of the SSHI circuit is compared against the standard rectifier, showing 183% and 134% power output enhancement for the first and second vibration modes, respectively.

* Author to whom any correspondence should be addressed.

Keywords: multimode energy harvesting, plate-like structure, piezoelectric, SSHI interface

(Some figures may appear in colour only in the online journal)

1. Introduction

Vibration energy is the most available ambient power source which can be harvested through several methods for powering small devices such as sensors and wireless electronics [1, 2]. Investigation of vibration-based energy harvesting has developed in past decades since it is an efficient alternative to conventional batteries and enables development of self-powered systems [3]. Among different methods for converting ambient vibration energy to electricity, piezoelectric materials are of great interest due to their remarkable power density and capability of manufacturing in desired geometries and scales [3, 4].

The geometry of the host structure for piezoelectric energy harvesters have taken various forms in the literature [4–6], where the cantilevered beams has been extensively investigated by researchers due to their relative simplicity of implementation [7–10]. However, the cantilever beam harvesters are strongly dependent on the narrow excitation frequency range, where the optimal performance typically happens at the primary resonance frequency. Consequently, if the vibration of ambient energy sources does not match the resonance frequency of the beam, the performance of the harvester drops drastically. Therefore, the application of cantilever beam harvesters is limited to controlled scenarios with specific excitation frequency. However, in practical applications, the vibration frequency spectrum of the environment is random and fluctuating [11]. Moreover, the cantilever beams have limited bandwidth characteristics for energy harvesting purposes, since the consecutive resonance frequencies are far from each other, hence broadband energy harvesting cannot be performed [12].

Recently, plate-like structures have drawn researchers' attention not only because of their availability in practical applications such as marine, aerospace, and automotive structures but also because of their capability of providing broadband energy harvesting systems due to their close consecutive resonance frequencies. Aridogan *et al* [13] presented an analytical solution and experimental validation for the plate-like piezo-patch energy harvesters with a resistive load as an external circuit which provides AC power output. The same research group pursued their research for a general case as multiple piezo-patch harvesters on a plate where the patches connected in parallel and series configurations satisfying the broadband energy harvesting through multiple vibration modes [14]. Improvement of estimation of the power output has been achieved considering the inertial and stiffness components of piezo-patches using Rayleigh–Ritz method [15].

In practice, stable power flow is required for electronic devices, hence DC output is more desirable and can be captured by using an AC to DC convertor circuit which has a nonlinear behavior [16]. The harvesting circuits including AC to DC convertor has been extensively studied where most investigations focused on the beam as the host structure [16–18]. Improvements on DC power output of the PEH can be achieved by adding a series connected switch and inductor to the rectifier. This technique is called synchronized switch harvesting on inductor (SSHI) [19–23]. During the vibration, the polarity of the piezo patch is inversed by triggering the switch only at the peak displacements of PEH. This artificial manipulation enhances the voltage generated by the piezoelectric element [19, 24]. Previous studies have presented an analytical solution for the SSHI circuit, which can estimate the power output of the harvester only at its resonance frequency [22, 25]. Furthermore, The difference in phase between the excitation and the mass velocity has also been taken into account in an improved analytical solution [24, 25]. The equivalent impedance approach has been proposed to obtain a closed form solution for rectifier, Parallel-SSHI, and Series-SSHI interfaces integrated with an array of piezoelectric energy harvesters connected in parallel [26] and in series [27] configuration. This approach is an approximation method and is based on simplifying the model to the fundamental harmonics of the system [28, 29]. New topologies of the self-powered SSHI circuit have been proposed to modify the peak detection units [22] and reduce the power loss of the circuit [30].

It has been proved that the harvesting circuit has a reaction to the dynamic of the host structure [31]. In practice, the more extracted power, the more induced damping effect [18]. However, the majority of the studies regarding the effect of the harvesting circuits on the dynamic of the structure are only focused on the cantilevered beams. Development of the models are carried out considering equivalent mass + springer + damper + piezo structure of the system around fundamental resonance frequency [2, 23, 24, 32, 33]. Despite all the advantages of plate-like structures for energy harvesting purposes i.e. availability in practical applications such as marine, aerospace, and automotive structures, and capability of providing broadband energy harvesting, the investigations on thin plate are limited to the simple harvesting circuits [4, 13–15]. A multi-mode equivalent circuit modeling of PEH integrated with standard harvesting circuit has been developed [34]. Moreover, analytical solution of wideband energy harvesting with multiple patches on a plate using a rectifier has been developed based on equivalent impedance approach [35]. A distributed-parameter model of a thin plate with multiple piezo-patches was developed based on standard modal analysis method. Piezoelectric metamaterial plate with local resonators integrated with synchronized charge extraction circuit was investigated to improve the performance of the harvesting system [36]. Despite all the

studies on the piezoelectric energy harvesting systems, the integration of self-powered SSHI circuit with piezoelectric energy harvester structurally coupled with a plate-like host structure is missing in the literature. The motivation of this paper is to study the energy harvesting performance of the self-powered SSHI circuit integrated with piezoelectric on a more available structure in practical applications i.e. plate with dense modal properties, and to compare the power extraction capability of the SSHI interface with the standard harvesting circuit. This system can be used in powering small electronic devices and structural health monitoring of 2D components in marine, aerospace, and automotive structures, as well as buildings.

In this paper, electromechanical equations of piezoelectric energy harvester on a thin plate are integrated with the equivalent load impedance of self-powered SSHI circuit for the first time, to predict the behavior of the harvesting system. Unlike the previous study [35], the effects of inertia and stiffness of piezoelectric are considered in this study. Due to discontinuities on the structure, Rayleigh–Ritz method is used to perform modal analysis and obtain natural frequencies and mode shapes of the structure. Besides, an experimental setup is developed to examine the harvesting performance of the SSHI circuit for the first and the second vibration modes of the host plate. Experimental results show that the SSHI circuit affects the dynamic of plate drastically in high resistive loads because of high modal density of thin plate. The effect of damping due to the SSHI interface is visible as ripples in the piezoelectric voltage waveforms. These ripples also change the switching behavior of the SSHI interface. An undesired multiple switching behavior of the SSHI circuit at high resistive load is observed which reduces the functionality of interface for energy harvesting purposes. It is shown that the analytical voltage outputs are in good agreement with the experimental results for the first and the second modes when there is just one switch in each half period of the vibration i.e. single switching. Besides, the experimental results show that the SSHI circuit does not switch at low piezoelectric voltage levels which means it is not active and behaves as a standard rectifier. A detailed study is carried out to show all these switching behaviors of the SSHI circuit along with the voltage and power output characteristics. Furthermore, it is demonstrated that the SSHI circuit improves the maximum DC output power of the harvester compared to a standard AC input-DC output (i.e. a standard rectifier) in both modes.

2. Analytical model

The analytical model of the electromechanical system consists of a thin plate with clamped boundary conditions for all four edges (CCCC) which is structurally integrated with a piezoelectric patch of thickness (h_{p}) connected to an SSHI interface (figure 1).

The piezoelectric patch is assumed to be perfectly bonded to the host structure. The model is based on Kirchhoff plate theory since the thickness of plate (h_s) is assumed to be much

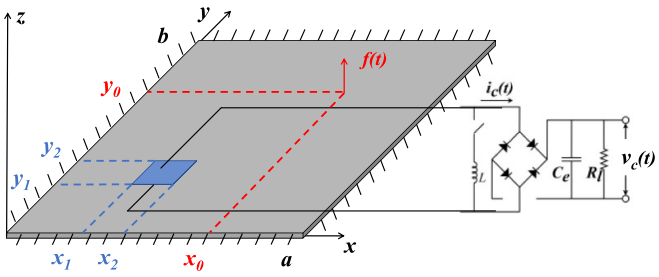

Figure 1. Schematic of the piezoelectric energy harvester attached to a thin plate.

smaller than the length (a) and width (b). Consequently, the piezoelectric energy harvester (PEH) is in a plane stress state, and the effect of transverse shear deformation can be neglected. It is assumed that the material of the host structure is isotropic. The material of the piezoelectric is transversely isotropic, and the direction of generated voltage is perpendicular to the applied strain. The model is developed for a transverse point force $f(t)$ which excites the plate at the position coordinates (x_0, y_0). The subscripts s and p stand for the parameters related to the host structure and piezoelectric patch. The Hamilton principle is used to derive the equation of motion which includes the effect of inertia and stiffness of the piezoelectric patch. The electromechanical equations of motion of PEH were previously developed by Yoon *et al* [15]. Due to the discontinuity of the geometry at the piezoelectric edges, the Rayleigh–Ritz method is implemented to conduct modal analysis and approximate the undamped natural frequencies and mode shapes of the model. The Rayleigh–Ritz method is based on discretizing the distributed-parameter model to obtain an approximation of the modal parameters. Linear combination of modes based on modal expansion theorem is considered to obtain an approximation of the displacement of PEH.

$$w(x,y,t) = \sum_{m=1}^{N}\sum_{n=1}^{N} \varphi_{mn}(x,y)\,.\eta_{mn}(t)\,. \tag{1}$$

where $\varphi_{mn}(x,y)$ is the mode shape and $\eta_{mn}(t)$ is the time dependent modal coordinate of the plate, for the mnth vibration mode ($m,\ n = 1, 2, \ldots, N$). N is a degree of approximation, and the convergence of natural frequencies happens when N is large enough. A set of N^2 electromechanical equations of motion can be written for PEH corresponding to N^2 degrees-of-freedom. Based on the orthogonality of modes, a set of N^2 independent equations of motion can be obtained by modal coordinate transformation. Differential equation of motion for a plate integrated with a piezo-patch in modal coordinate is [15]

$$\frac{\mathrm{d}^2\eta_{mn}(t)}{\mathrm{d}t^2} + 2\zeta_{mn}\omega_{mn}\frac{\mathrm{d}\eta_{mn}(t)}{\mathrm{d}t} + \omega_{mn}^2\eta_{mn}(t) - \Theta_{mn}v_{\mathrm{p}}(t) = f_{mn}(t) \tag{2}$$

where $v_{\mathrm{p}}(t)$ is the piezoelectric voltage, ω_{mn} is the undamped natural frequency and ζ_{mn} is the modal damping ratio for

the *mn*th vibration mode. Θ_{mn} corresponds to the modal electromechanical coupling of the piezoelectric patch for *mn*th vibration mode and is defined as [15]:

$$\Theta_{mn} = -\bar{e}_{31}\left(\frac{h_p + h_s}{2} - z_0\right)\int_{y1}^{y2}\int_{x1}^{x2}\left[\frac{\partial^2\varphi_{mn}(x,y)}{\partial x^2} + \frac{\partial^2\varphi_{mn}(x,y)}{\partial y^2}\right]\mathrm{d}x\mathrm{d}y. \quad (3)$$

where $\bar{e}_{31}$ is piezoelectric constant, and $\varphi_{mn}(x,y)$ is the mass normalized eigenfunction of the plate for *mn*th vibration mode. $z_0$is the location of the neutral surface in the areas in which the piezoelectric patch is attached. Modal forcing input which corresponds to the force for each mode shape is denoted by $f_{mn}(t)$ and is given by [35]

$$f_{mn}(t) = f(t)\,\varphi_{mn}(x_0, y_0)\,. \quad (4)$$

Equivalent circuit of a piezoelectric device can be presented as its internal electrode capacitance C_p in parallel with a set of parallel branches of second order LCR circuit which is equivalent to a velocity proportional current source (figure 2) where $C_\mathrm{p} = \bar{\varepsilon}_{33}^{S}\frac{l_\mathrm{p}{}^{*}w_\mathrm{p}}{h_\mathrm{p}}$ and $\bar{\varepsilon}_{33}^{S}$, l_p, w_p and $h_\mathrm{p}$are the permittivity at constant strain, length, width, and thickness of piezoelectric patch, respectively [15].

The coupled circuit equation of piezoelectric is

$$C_\mathrm{p}\frac{\mathrm{d}v_\mathrm{p}(t)}{\mathrm{d}t} + i_c(t) = i_p(t) \quad (5)$$

where $i_p(t)$ and $i_c(t)$ are the equivalent current source, and the current flowing into the SSHI circuit, respectively. It is worth noting that all the AC to DC circuits affect the behavior of the harvesting system. However, it can be assumed that the impact of the higher order harmonics due to the self-powered SSHI circuit is negligible compared to the fundamental component. Consequently, the model can be simplified where the equivalent current source $i_p(t)$ can be assumed to be perfectly harmonic, and piezoelectric voltage $v_\mathrm{p}(t)$ can be regarded as its fundamental harmonic [29]. The electrical equation in modal coordinates can be presented as [15]

$$-\sum_{\mathrm{m}=1}^{\mathrm{N}}\sum_{\mathrm{n}=1}^{\mathrm{N}}\Theta_{mn}\frac{\mathrm{d}\eta_{mn}(t)}{\mathrm{d}t} + i_c(t) + C_\mathrm{p}\frac{\mathrm{d}v_\mathrm{p}(t)}{\mathrm{d}t} = 0. \quad (6)$$

Equivalent current source of piezoelectric harvester can be obtained from equations (5) and (6), as follows,

$$i_p(t) = \sum_{m=1}^{N}\sum_{n=1}^{N}\Theta_{mn}\frac{\mathrm{d}\eta_{mn}(t)}{\mathrm{d}t}\,. \quad (7)$$

3. Equivalent impedance approach

SSHI harvesting interface refers to an inductance L connected in series with a switch which is in parallel with a rectifier bridge and piezoelectric patch (figure 2).

The switch is always open except in time instant of extremum displacement. When the switch is triggered, the

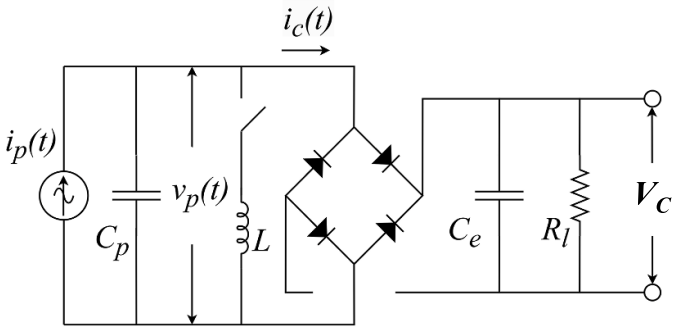

Figure 2. Equivalent circuit of a piezoelectric device.

inductance L and capacitance of piezoelectric C_p form an oscillator circuit which reverses the voltage of the piezoelectric element. The inversion process consists of an energy loss in the inductor and the switch, therefore, an inversion quality factor Q_I can be defined for the SSHI circuit. Solving the electromechanical equations for the SSHI circuit integrated with a piezoelectric patch on a plate structure is not straight forward since the circuit consists of electrical components such as diodes and switches. Therefore, an equivalent impedance approach is used to solve the electromechanical equations.

Considering a transverse point force of $f(t) = F_0 e^{i\omega t}$ as harmonic input at frequency ω, and approximate the piezoelectric voltage with its fundamental harmonic ($v_\mathrm{p}(t) = V_\mathrm{p}e^{i\omega t}$), the steady-state response of the system based on linear system assumption can be expressed as

$$\eta_{mn}(t) = H_{mn}e^{i\omega t} \quad (8)$$

where H_{mn} and V_p are complex numbers. Inserting $f(t)$, equations (4), and (8) into (2), the complex modal response H_{mn} can be expressed as

$$\mathrm{H}_{mn} = \frac{F_0\varphi_{mn}(x_0,y_0) + V_p\Theta_{mn}}{\omega_{mn}^2 - \omega^2 + i2\zeta_{mn}\omega_{mn}\omega}\,. \quad (9)$$

Inserting (8) into (7), steady-state form of velocity proportional current source of piezoelectric can be expressed as $i_p(t) = I_\mathrm{p}e^{i\omega t}$ where the complex amplitude is

$$I_\mathrm{p} = \sum_{m=1}^{N}\sum_{n=1}^{N}I_{mn} = \sum_{m=1}^{N}\sum_{n=1}^{N}\left[i\omega\Theta_{mn}\mathrm{H}_{mn}\right]\,. \quad (10)$$

The relation between the magnitude of the equivalent piezoelectric current source and the average output voltage can be calculated by [23]

$$V_c = \frac{2R_l}{\pi + (1-q_I)\,C_\mathrm{p}\omega R_l}I_\mathrm{p}. \quad (11)$$

Where q_I is the ratio of the piezoelectric voltage after switching and before switching ($q_\mathrm{I} = \frac{V_\mathrm{p}^{\ \mathrm{after}}}{V_\mathrm{p}^{\ \mathrm{before}}} = e^{-\frac{\pi}{2Q_I}}$) and Q_I is the inversion quality factor of the SSHI circuit. To obtain output voltage, let Z_eq be the equivalent impedance of the SSHI circuit plus piezoelectric capacitance as shown in figure 3.

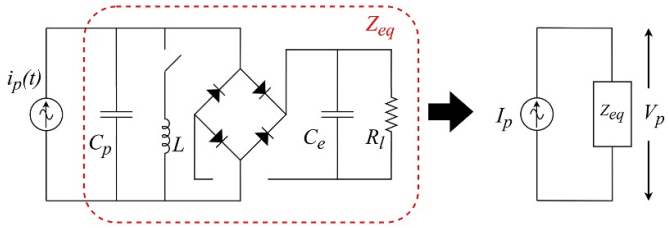

Figure 3. Equivalent impedance of a piezoelectric energy harvester integrated with SSHI interface.

For array of SDOF harvesters connected in parallel to the SSHI circuit, equivalent impedance model has been proposed as a function of resistive load R_l, capacitance of piezoelectric C_p, and excitation frequency ω [26]. Equivalent impedance is a complex value ($Z_\mathrm{eq} = Z_R^{\mathrm{SSH}} + jZ_I^{\mathrm{SSHI}}$) which is expressed as

$$Z_R^{\mathrm{SSHI}} = \frac{2R_l\left[1+\frac{(1-q_l^2)}{2\pi}C_\mathrm{p}\omega R_l\right]}{\left(\frac{\pi}{2}+\frac{(1-q_l)}{2}C_\mathrm{p}\omega R_l\right)^2},\ Z_I^{\mathrm{SSHI}} = \frac{-\frac{(1-q_l)}{2}R_l}{\left(\frac{\pi}{2}+\frac{(1-q_l)}{2}C_\mathrm{p}\omega R_l\right)}. \tag{12}$$

The relation between the current flowing into Z_eq and the voltage across it can be expressed as

$$V_\mathrm{p} = Z_\mathrm{eq}I_\mathrm{p} = Z_\mathrm{eq}\sum_{m=1}^{N}\sum_{n=1}^{N}I_{mn}\,. \tag{13}$$

Substituting $v_\mathrm{p}(t)$, equations (8), and (13) into (2) and dividing both sides by the Θ_{mn}, the mechanical equation of piezoelectric harvester can be obtained as

$$\left(\omega_{mn}^2-\omega^2+i2\zeta_{mn}\omega_{mn}\omega\right)\frac{\mathrm{H}_{mn}}{\Theta_{mn}} - Z_\mathrm{eq}I_\mathrm{p} = F_0\frac{\varphi_{mn}(x_0,y_0)}{\Theta_{mn}}. \tag{14}$$

Inserting equation (10) as the steady-state form of velocity proportional current source into equation (14), it can be showed that the equation can be expressed by the matrix equation as [37]

$$\widehat{\boldsymbol{V}} = \widehat{\boldsymbol{Z}}\widehat{\boldsymbol{I}} \tag{15}$$

where $\widehat{\boldsymbol{V}}$ is a vector of dimension $mn \times 1$ and can be calculated as

$$\begin{aligned}&\hat{\boldsymbol{V}} = \left(\hat{V}_{kl}\right) = -F_0\tfrac{\varphi_{kl}(x_0,\,y_0)}{\Theta_{kl}},\\ &k\ =1,\,2,\ldots,m;\ l=1,\,2,\ldots,n\end{aligned} \tag{16}$$

and $\widehat{\boldsymbol{Z}}$ as a square matrix of dimension $mn \times mn$ is given by $\widehat{\boldsymbol{Z}} = Z_\mathrm{eq}\boldsymbol{A} + \mathrm{diag}(\boldsymbol{Z})$. Matrix $\boldsymbol{A}$ is of dimension $mn \times mn$ with all elements equal to one, and $\mathrm{diag}(\boldsymbol{Z})$ is a diagonal matrix, where its diagonal elements are $\boldsymbol{Z} = [Z_{11}\ Z_{21}\ldots\ Z_{mn}]^\mathrm{T}$ and is obtained by

$$\begin{aligned}&Z_{kl} = \frac{2\zeta_{kl}\omega_{mn}}{(\Theta_{kl})^2} + i\frac{\omega^2-\omega_{kl}^2}{\omega(\Theta_{kl})^2},\quad .\\ &k=1,2,\ldots,m;\ l=1,2,\ldots,n\end{aligned} \tag{17}$$

Solving equation (15) for the unknown $\widehat{\boldsymbol{I}}$ which includes I_{mn} as magnitude of equivalent current for each oscillating mode and inserting it into (11), the output voltage of the SSHI circuit can be extracted. Consequently, the DC power output of the harvester can be estimated by

$$P_c = \frac{{V_c}^2}{R_l}\,. \tag{18}$$

Moreover, the complex modal response H_{mn} can be determined by (14). Thus, the mechanical modal coordinate $\eta_{mn}(t)$ is obtained, and transverse displacement of the plate at any point of $(x,\,y)$ as a function of time can be obtained by

$$\begin{aligned}w(x,y,t) &= \sum_{m=1}^{N}\sum_{n=1}^{N}\varphi_{mn}(x,y)\,.\eta_{mn}(t)\\ &= \sum_{m=1}^{N}\sum_{n=1}^{N}\left\{\frac{\varphi_{mn}(x,y)}{\omega_{mn}^2-\omega^2+i2\zeta_{mn}\omega_{mn}\omega}.\left(F_0\varphi_{mn}(x_0,y_0)\right.\right.\\ &\quad\left.\left.+\Theta_{mn}Z_{eq}\sum_{m=1}^{N}\sum_{n=1}^{N}I_{mn}\right)\right\}.e^{i\omega t}.\end{aligned} \tag{19}$$

4. Model validations

4.1. Experimental setup

Experimental setup consists of a fully clamped (CCCC) aluminum plate which has been excited by a linear sine point force located at 0.087 and 0.087 m away from the bottom right corner of the plate in x and y directions, respectively. The piezo-patch harvesters (T105-A4E-602 manufactured by Piezo Systems, Inc.) were bonded on the aluminum plate (figure 4), where the piezo patch on the left side has been used as the harvester and two other patches have been short circuited to eliminate the backward piezoelectric effect.

Table 1 introduces the geometric, mechanical, and electroelastic properties of the experimental setup. A force transducer (PCB 208C02) was installed at the tip of the shaker to measure the dynamic force which is the reference input of the system and was used to determine the voltage frequency response function (FRF) of the harvester. A laser Doppler vibrometer (Polytec PDV 100) measured the transvers velocity output of the plate. A resistance box which provides a wide range of resistance from 1 Ω through 1 MΩ has been used to generate desired resistive load. The experiments were conducted considering three different harvesting circuits, i.e. resistive load, standard rectifier, and SSHI circuit (figure 5). The aim of conducting the AC input-AC output experiment with resistive load was determination of modal damping ratios of the structure and initial validation of the model. On the other hand, a standard rectifier was used to assess the harvesting performance of the SSHI, since they both aim to extract DC power output. The SSHI circuit used in the experiment and the schematic of the circuit is available in figure 6. The operation principle of this self-powered SSHI circuit was fully detailed in [30].

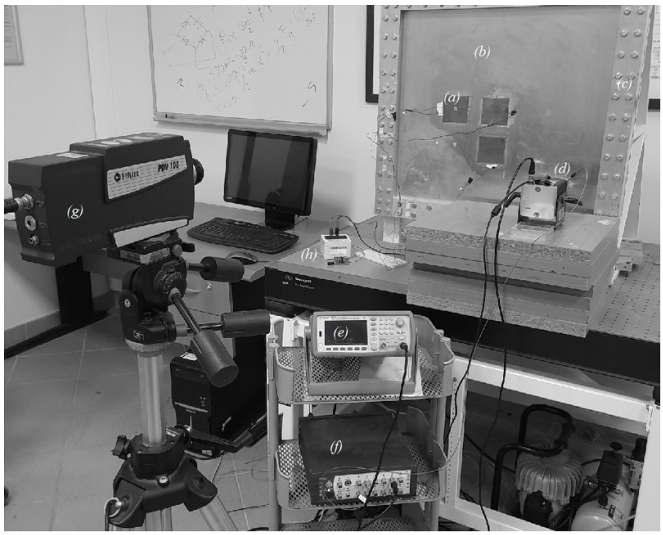

Figure 4. Experimental setup: (a) PZT; (b) aluminum plate; (c) clamping frame; (d) shaker and a force transducer; (e) signal generator; (f) data acquisition unit; (g) laser vibrometer; and (h) electrical circuit.

Table 1. Dimension and material properties of the plate and the piezo patch.

Property	Aluminum	Piezoceramic
Length (mm) X	580	72.4
Width (mm) Y	540	72.4
Thickness (mm)	1.9	0.267
Young's modulus (GPa)	65.1	66
Mass density (Kg m^{-3})	2575	7800
Piezoelectric constant (pm V^{-1})	—	−190
Permittivity constant (nF m^{-1})	—	10.38

4.2. Experimental validation for AC input-AC output

In the case of resistive load as harvesting circuit, a sine signal was swept over a frequency range of 40–115 Hz to measure the voltage frequency response function (FRF) of the system which was used to identify the modal damping ratios of the structure. The experimental voltage FRFs for any resistive load can be used to extract the modal damping ratios of the system [3]. The voltage FRFs of the harvester for AC input-AC output case with two resistive loads satisfying short circuit ($R_l = 100\Omega$) and open circuit ($R_l = 1\text{M}\Omega$) condition is shown in figure 7.

As shown in figure 7 the analytical voltage FRF prediction accurately matches with the experimental result. Comparing the experimental and analytical results, the predicted natural frequencies of the model have 3.8%, and 1.7% errors for the first and the second vibration modes of the system. It is worth mentioning that providing an ideal clamping condition for the plate structure in the experimental setup is difficult to achieve and any possible discrepancy in the boundary conditions can affect the modal parameters of the structure. Besides, the experimental room conditions specially the temperature can affect the natural frequencies of the plate

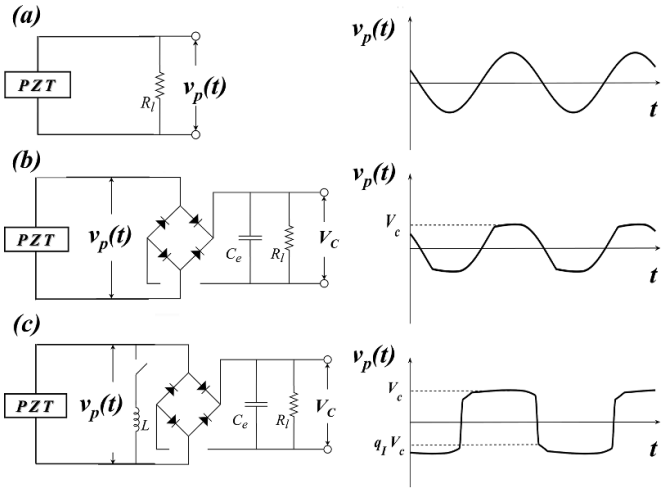

Figure 5. Piezoelectric voltage waveforms for (a) resistor, (b) rectifier, and (c) SSHI.

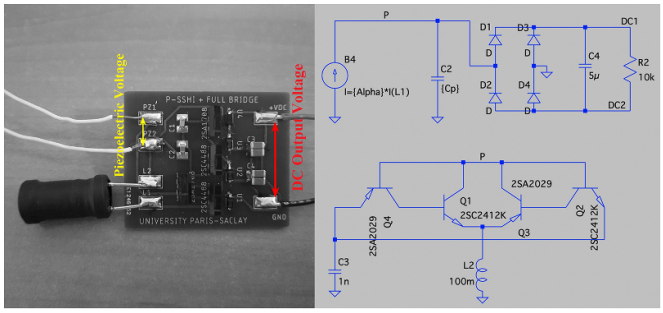

Figure 6. SSHI circuit and its schematic.

[38]. Moreover, the material properties used in the analytical model are obtained from the standard tables of the aluminum alloy used in this experiment. However, there may be a difference between the actual values and the reported ones in the standards.

4.3. Experimental validation for AC input-DC output with standard rectifier circuit

For the sake of comparison with the SSHI circuit, the DC response of PEH with rectifier circuit in frequency domain was obtained by sweeping the frequency of the harmonic excitation around two first natural frequencies of the harvester. The sweeping time of the swept sine signal has been kept long enough to capture the steady state response of the system and short enough to avoid huge experiment data (sweep-time = 180 (s)). The voltage response of the rectifier for 13 resistive loads ranging from 1KΩ through 1MΩ around two first natural frequencies of the plate was measured. The results of seven resistive loads are presented in figure 8. Peak voltage response of the analytical model for several resistive loads has maximum error of 5.3% in the first vibration mode and 9% in the second vibration mode when compared with the experimental results. Although the voltage loss and the real diode

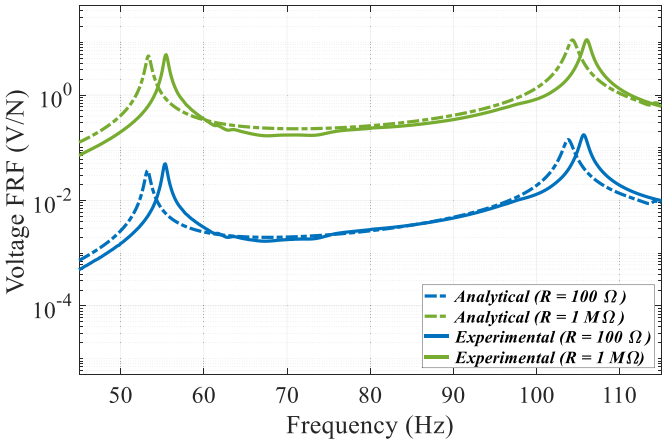

Figure 7. Comparison of analytical and experimental voltage FRFs for AC input-AC output.

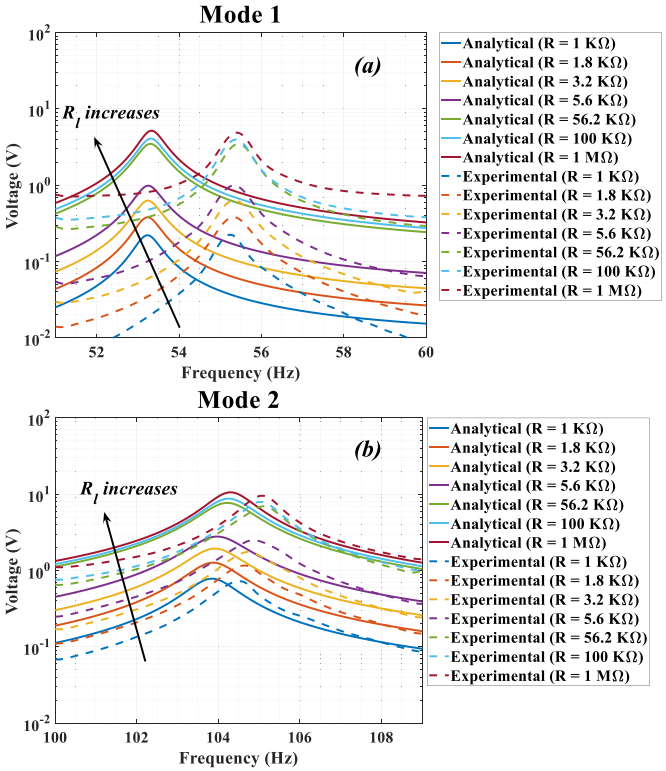

Figure 8. Analytical results and experiment data for DC output voltage of rectifier circuit under 1 N excitation force. (a) First vibration mode; (b) second vibration mode.

behavior are not included in the analytical model, the analytical model results reasonably follow the trend of the experimental voltage response where the voltage difference is less than 0.3 (V) and 0.9 (V) for the first and the second modes, respectively.

4.4. Experimental validation for AC input-DC output with SSHI circuit

The aluminum plate with piezo patches was excited by a sine signal to obtain the harmonic response of the system for several resistive loads and assess the performance of the

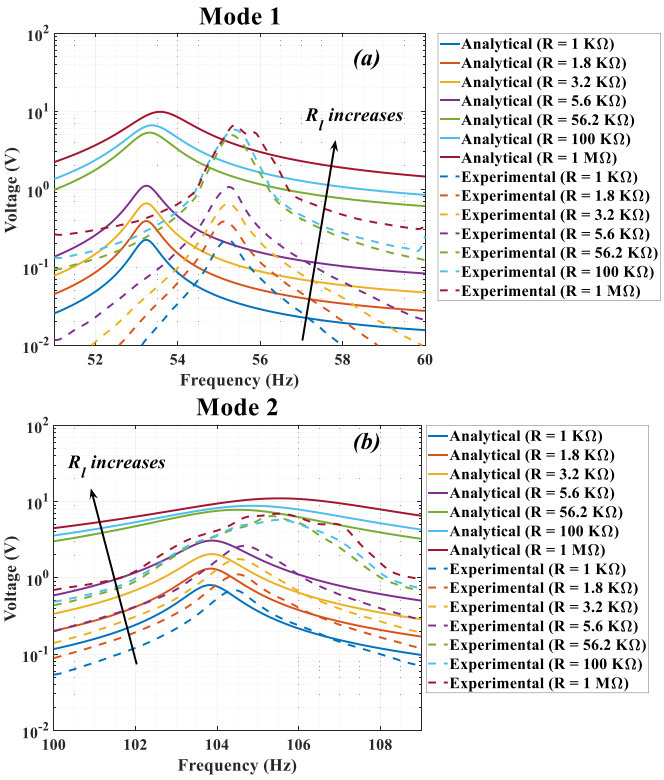

Figure 9. Analytical results and experiment data for DC output voltage of SSHI circuit under 1 N excitation force. (a) First vibration mode; (b) second vibration mode.

SSHI circuit when integrated with piezoelectric on the plate like host structure. The excitation frequency has been swept over a frequency range around the two first natural frequencies of the system considering an appropriate sweeping time (180 (s)) which provides enough charge time for the smoothing capacitor and prevents large acquisition data due to high sampling rate. The quality factor of the SSHI circuit is 3.21. The output voltage of the SSHI circuit for 13 resistive loads are measured and seven of them are compared with the analytical results in figure 9. Experimental results show that the SSHI response resembles the response of the rectifier for the resistive loads of 1, 1.8, and 3.2 KΩ in the first mode, and for the resistive loads of 1 and 1.8 KΩ in the second mode. Studying the experimental piezoelectric voltage waveforms of the SSHI circuit which shows the behavior of the interface for different resistive loads (figures 10 and 11) comes up with the fact that the SSHI does not switch in low resistive loads since the piezoelectric voltage level is not sufficient to run the switching phenomena, and the SSHI circuit acts as a rectifier.

It also can be seen in figure 9 that the analytical model results follows the trend of the experimental data for the resistive loads between 5.6 KΩ and 100 KΩ in the first mode, and for the resistive loads between 3.2 KΩ and 56.2 KΩ in the second mode. In this range of resistive loads, the voltage difference between the analytical prediction and the experimental result for the peak voltage values are less than 0.55 (V) and 1.18 (V) in the first mode and the second mode, respectively.

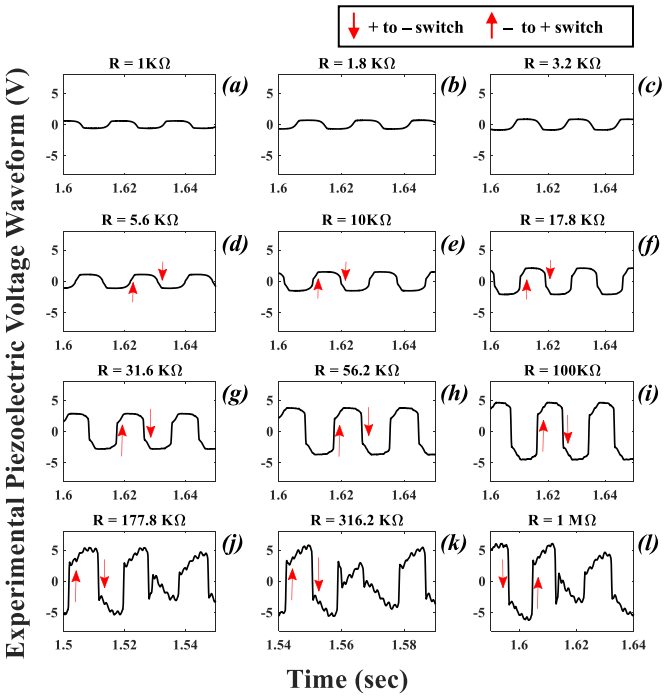

Figure 10. Experimental piezoelectric voltage waveforms (before the SSHI circuit) in the first vibration mode for different resistive loads. Indicate with (a)–(c) no switching … (d)–(i) single switching …, and (j)–(l) multiple switching.

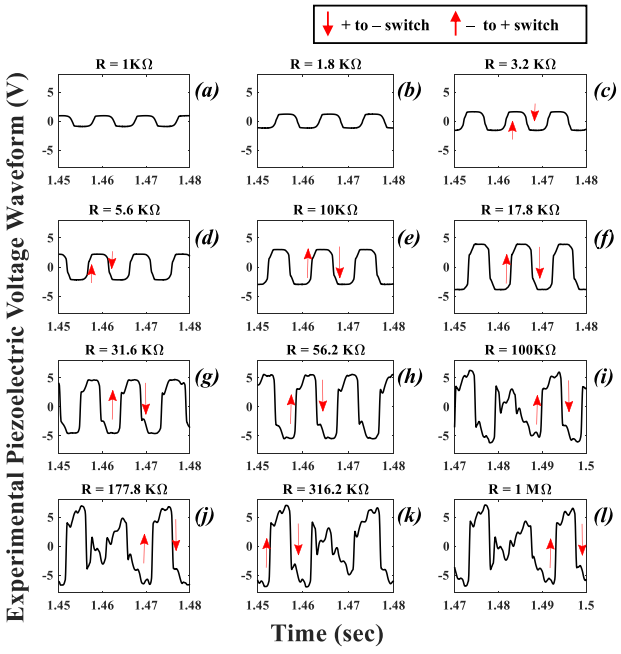

Figure 11. Experimental piezoelectric voltage waveforms (before the SSHI circuit) in the second vibration mode for different resistive loads. Indicate with (a) and (b) no switching … (c)–(h) single switching …, and (i)–(l) multiple switching.

The voltage loss of the circuit components such as diodes and switching unit has not been included in the analytical model; however, the analytical model reasonably follows the trend of

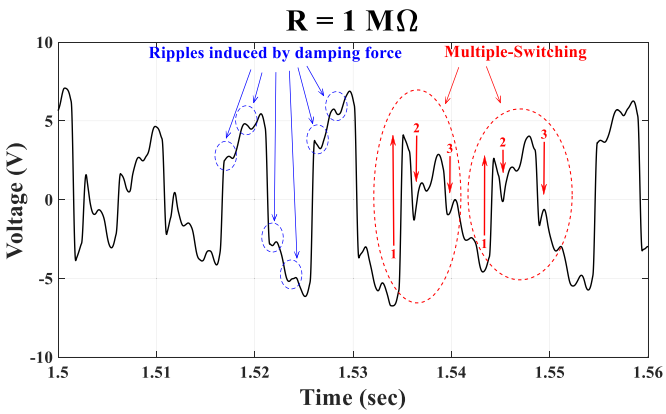

Figure 12. Multiple switching and ripple creation in piezoelectric voltage waveforms of second vibration mode ($\omega = 55.2$ Hz) for 1 MΩ resistive load.

experimental results. The experimental piezoelectric voltage waveforms show that the SSHI circuit has a single switch in each half period of the vibration for this range of resistive loads which is the expected and the optimal behavior of the SSHI circuit.

Moreover, the voltage output of the SSHI for the resistive loads higher than 100 KΩ in the first mode, and for the resistive loads higher than 56.2 KΩ in the second mode does not follow the trend of the analytical prediction (figure 9). The equivalent impedance of the harvesting circuit is based on the fundamental harmonic of the SSHI circuit [29]; however, higher order harmonics for high resistive loads are significant and can be seen as ripples in the experimental piezoelectric voltage waveforms (figures 10 and 11). Therefore, the analytical model is not capable of predicting the trend of system behavior for high resistive loads. The voltage difference between the analytical model and experiment is more than 1.75 (V) in first mode and more than 3.3 (V) in the second mode.

It is worth noting that dense modal properties of the plate make the higher order harmonics become significant. The SSHI circuit affects the dynamic of plate by inducing a damping force which is considerable in higher voltage levels. When the frequency spectrum of the damping force coincides with the higher vibration modes of the plate, it induces an extra resonance to the dynamic of the plate and cause some ripples in the piezoelectric voltage waveforms (figure 12). If the ripples are large enough, the multiple switching happens since the SSHI circuit detects them as local extrema and triggers the switch. Multiple switching dissipates a part of available energy and reduces the optimality of the SSHI interface. However, the multiple switching does not happen in optimum resistive loads. This behavior can be avoided or reduced by considering higher order harmonics of plate-like structure as a design parameter of the SSHI circuit and select appropriate inductance for the switching device.

Perfect performance of the SSHI circuit consists of switching the piezo-patch voltage at extremum displacement of the plate i.e. zero velocity of the plate. However, in practice, the switching process happens with a positive or negative time

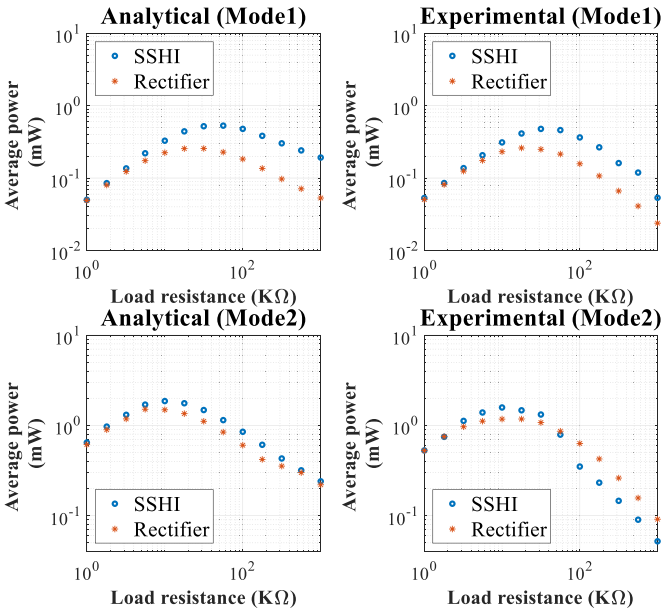

Figure 13. Analytical and experimental results for average power output of the SSHI and rectifier circuits.

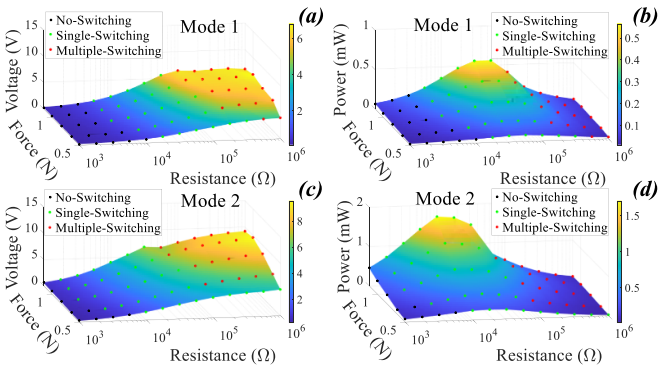

Figure 14. DC voltage and power output of the SSHI circuit for different input force levels and resistive loads (a) and (c) first vibration mode ($\omega = 55.2$ Hz), (b) and (d) second vibration mode ($\omega = 104.5$ Hz).

delay which can reduce the power output of the harvesters. The effect of switching delay depends on mechanical quality factor (Q_M) and electromechanical coupling factor (k^2) of the system. As it is shown in appendix (figure 15), the SSHI device used in this study has positive switching delay. Considering the (k^2) and (Q_M) of the system, it can be concluded that the switching delay does not have significant effect on the power output of the harvesting system. Details of the switching delay and parameters of the system are available in the appendix.

The experimental data and analytical prediction of the peak power output as a function of resistive loads for the SSHI circuit and the rectifier are compared in figure 13. Analytical results illustrate that the optimum resistive load for rectifier in the first mode is 31.6 kΩ while it is 56.2 kΩ for SSHI circuit, and the respective average power output is 0.25 (mW) and 0.53 (mW) for rectifier and SSHI circuit, respectively. Also, the optimum resistance for the analytical power output of the SSHI and the rectifier in the second mode is 10 kΩ and 5.6 kΩ, respectively which leads to 1.86 (mW) and 1.51 (mW) power output, respectively. The analytical results show that the power output of the SSHI circuit at optimum resistance is 207% of the rectifier in the first mode and 124% in the second mode. On the other hand, the experimental data in the first mode shows that the maximum power output of the SSHI can be achieved at 31.6 kΩ where it is 17.8 kΩ for the rectifier. The maximum power output obtained from experiment in the first mode for the SSHI is 0.4779 (mW) while it is 0.26 (mW) for the rectifier. Besides, the maximum power output of experimental results in the second mode is 1.58 (mW) for SSHI circuit with 10 KΩ resistive load and 1.177 (mW) for rectifier with 17.8 KΩ resistive load. The Experimental power output of the SSHI circuit is 183% and 134% of the rectifier for mode one and mode two, respectively. The analytical results and experimental data for the first vibration mode show that the SSHI circuit improves the power output of the harvester for all resistive loads except where it is not active. Although the power output of the harvester in the second vibration mode is improved by the SSHI circuit in optimum resistive load, the analytical and experimental results show that the SSHI circuit is not effective for relatively high resistive loads in second mode. The analytical model is only capable of predicting the linear regime where single switching at each half period of vibration occurs, but the model cannot predict the nonlinearities of experimental setup at high resistive loads. The multiple switching reduces the power output of the system which is more visible at second vibration mode. The power reduction due to multiple switching at second vibration mode reduces the performance of the SSHI circuit even lower than standard rectifier.

A comprehensive experiment has been performed to assess the behavior of the SSHI circuit for different input force levels, and resistive loads. Thirteen resistive loads between 1 KΩ and 1 MΩ with logarithmic increments and force levels, namely 0.5, 65, 82, 1, and 1.15 (N), have been considered to study the response of the piezoelectric energy harvester integrated with the SSHI circuit. The DC voltage output of the PEH in the first vibration mode (figure 14(a)) and the second vibration mode (figure 14(b)) show that the higher the input gain and the resistive load, the higher the DC voltage output. However, this trend is more visible in single switching areas, and the rate of voltage increase is dropped in multi-switching zone which shows that the performance of the SSHI circuit is not efficient. Therefore, multi-switching should be avoided to make the SSHI circuit reach its optimal performance. Besides, the DC output voltage level of 1.5 V is a threshold for triggering the switch, where the DC voltage levels higher than 5 V experience the multi-switching. Regarding the power output of PEH, the optimum resistive loads of different force inputs are available in figures 14(c) and (d) for mode 1 and mode 2, respectively. The optimum resistive load of almost all the cases in the first mode is 31.6 KΩ, and in the second mode is 10 KΩ.

5. Conclusion

In this paper, an analytical model was developed to predict the behavior of a piezoelectric energy harvester on a thin plate integrated with an SSHI circuit. Structural analysis was performed based on Rayleigh–Ritz method to obtain an electromechanical model of the plate with PEH, and the equivalent impedance approach was used to provide a closed-form solution for the system. The steady-state voltage output of the piezoelectric energy harvester for a range of resistive loads around first and second natural frequencies were predicted by analytical solution and validated by the experimental data where the SSHI circuit had single switching in each half period of the vibration. A comprehensive analysis of the SSHI circuit behavior on the plate for different force inputs and resistive loads was investigated and presented. Using a 2D electromechanical plate, multi-switching of the SSHI circuit in higher piezoelectric voltage levels was observed. Multiple switching increased the energy dissipation of the harvesting circuit; thus, the output voltage of the harvester dropped drastically when compared to the analytical prediction. Furthermore, the peak power output of the SSHI circuit as a function of resistive load was compared with the rectifier for the first two vibration modes of the plate to assess the functionality of the SSHI circuit in multimodal energy harvesting applications. It has been demonstrated that the SSHI circuit improves the power output of the PEH for both vibration modes in optimum resistive loads. Practically, the maximum power outputs of the SSHI circuit for the first and the second vibration modes were 183% and 134% of the maximum power outputs of the rectifier, respectively.

Despite improvements on maximum power output of the piezoelectric energy harvester by the SSHI circuit, undesired behavior of the switching device is reported when the PEH is attached to the plate-like structure. The developed equivalent impedance model can predict the linear regime of SSHI circuit, where the single switching occurs at each half period of vibration. At high resistive loads leading to higher voltage levels, higher modal harmonics of the host plate are coupled with switching dynamics of SSHI circuit. In order to avoid multiple switching behavior of the SSHI circuit, it is worthful to consider the higher order harmonics of the plate-like structure as a design parameter. The value of inductor on switching device should satisfy the synchronized switching criteria as well as avoiding the multiple switching behavior of SSHI circuit when integrated with plate-like structures. Adding filters in the peak voltage detector of the switching device is another approach that could be investigated to avoid performance drop resulting from multiple switching.

Data availability statement

All data that support the findings of this study are included within the article (and any supplementary files).

Acknowledgments

We acknowledge the financial support provided by the Scientific and Technological Research Council of Turkey (TUBITAK).

Funding

This work was supported by the Scientific and Technological Research Council of Turkey TUBITAK.

Appendix

The ideal performance of the SSHI circuit is the triggering the switch at the zero velocity of the PEH. Yet, in practical applications, there is a negative or positive time delay between the actual occurrence of zero velocity and the inversion. Negative switching delay corresponds to the triggering of the switch before reaching the zero velocity, where positive delay refers to the switching after the zero velocity [39]. It is proved in [39] that the power reduction level depends on the sign of delay, length of delay, and figure of merit (FoM). FoM is defined as the product of mechanical quality factor (Q_{M}) and the global electromechanical coupling factor (k^2). The mechanical quality factor depends on the modal damping ratio (ζ_{mn}) and is defined as:

$$Q_{\mathrm{M}} = \frac{1}{2\zeta_{mn}}. \tag{20}$$

The electromechanical coupling factor can be calculated by

$$k^2 = 1 - \frac{\omega_{\mathrm{sc}}^2}{\omega_{\mathrm{oc}}^2} \tag{21}$$

where the $\omega_{\mathrm{sc}}$and ω_{oc}represent the short circuit and open circuit resonance frequencies.

The voltage and velocity waveforms of piezo patch (figure 15) illustrate that the SSHI circuit has positive switching delay which does not have significant effect on output power for a large range of time delay. The power drop of the harvester has been studied by Lallart *et al* [39] for five values of FoM varying from FoM = 0.1877 as weakly coupled and FoM = 3.1845 as strongly coupled harvesters, and it has been shown that the power drop in the positive switching delay decreases by increasing the FoM. The parameters of the energy harvester integrated with the SSHI circuit for the first and the second vibration modes are available in table 2.

Comparing the FoM = 0.982 and FoM = 1.81, respectively, for the first and the second vibration modes of the system with the results of Lallart *et al* [39], and considering the positive time delay ratio less than 0.03 of vibration period for both modes, the power drop of the harvester due to the switching delay can be negligible for the SSHI circuit.

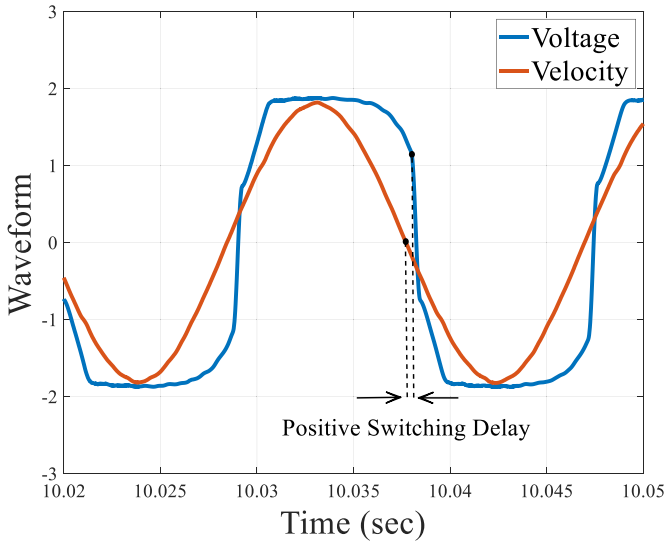

Figure 15. Piezoelectric voltage and velocity waveform in the first resonance frequency ($\omega = 55.2$ Hz).

Table 2. The parameters of the energy harvester integrated with the SSHI circuit.

Parameter	Mode 1	Mode 2
ω_{sc} (Hz)	53.22	103.81
ω_{oc} (Hz)	53.51	104.84
ζ_{mn}	0.0055	0.0054
k^2	0.010 81	0.019 55
Q_M	90.9	131.57
FoM	0.982	1.810

ORCID iDs

Seyed Morteza Hoseyni https://orcid.org/0000-0002-9057-1223
Mehmet Simsek https://orcid.org/0000-0002-8736-2586
Amirreza Aghakhani https://orcid.org/0000-0002-4301-4053

References

[1] Safaei M, Sodano H A and Anton S R 2019 A review of energy harvesting using piezoelectric materials: state-of-the-art a decade later (2008–2018) *Smart Mater. Struct.* **28** 113001
[2] Liao Y and Liang J 2019 Unified modeling, analysis and comparison of piezoelectric vibration energy harvesters *Mech. Syst. Signal Process.* **123** 403–25
[3] Erturk A and Inman D J 2011 *Piezoelectric Energy Harvesting* (Wiley)
[4] Aridogan U, Basdogan I and Erturk A 2013 Electroelastic finite element modeling and experimental validation of structurally-integrated piezoelectric energy harvester *Int. Design Engineering Technical Conf. and Computers and Information in Engineering Conf.* vol 55997 (American Society of Mechanical Engineers) p V008T13A089
[5] Xie X, Wang Z, Liu D, Du G and Zhang J 2020 An experimental study on a novel cylinder harvester made of L-shaped piezoelectric coupled beams with a high efficiency *Energy* **212** 118752
[6] Ahmad M R, Khan M R A A and Rahman M A 2016 Energy harvesting based on cantilever beam for different piezoelectric materials from acoustic vibration by simulation process *2016 9th Int. Conf. on Electrical and Computer Engineering (ICECE)* (IEEE) pp 318–20
[7] Erturk A and Inman D J 2008 A distributed parameter electromechanical model for cantilevered piezoelectric energy harvesters *J. Vib. Acoust.* **130** 041002
[8] Erturk A and Inman D J 2009 An experimentally validated bimorph cantilever model for piezoelectric energy harvesting from base excitations *Smart Mater. Struct.* **18** 025009
[9] Cottone F, Gammaitoni L, Vocca H, Ferrari M and Ferrari V 2012 Piezoelectric buckled beams for random vibration energy harvesting *Smart Mater. Struct.* **21** 035021
[10] Zheng X, Zhang Z, Zhu Y, Mei J, Peng S, Li L and Yu Y 2015 Analysis of energy harvesting performance for d_{15} mode piezoelectric bimorph in series connection based on timoshenko beam model *IEEE/ASME Trans. Mechatronics* **20** 728–39
[11] Tang L, Yang Y and Soh C K 2010 Toward broadband vibration-based energy harvesting *J. Intell. Mater. Syst. Struct.* **21** 1867–97
[12] Erturk A, Renno J M and Inman D J 2009 Modeling of piezoelectric energy harvesting from an l-shaped beam-mass structure with an application to UAVs *J. Intell. Mater. Syst. Struct.* **20** 529–44
[13] Aridogan U, Basdogan I and Erturk A 2014 Analytical modeling and experimental validation of a structurally integrated piezoelectric energy harvester on a thin plate *Smart Mater. Struct.* **23** 045039
[14] Aridogan U, Basdogan I and Erturk A 2014 Multiple patch–based broadband piezoelectric energy harvesting on plate-based structures *J. Intell. Mater. Syst. Struct.* **25** 1664–80
[15] Yoon H, Youn B D and Kim H S 2016 Kirchhoff plate theory-based electromechanically-coupled analytical model considering inertia and stiffness effects of a surface-bonded piezoelectric patch *Smart Mater. Struct.* **25** 025017
[16] Shu Y and Lien I 2006 Analysis of power output for piezoelectric energy harvesting systems *Smart Mater. Struct.* **15** 1499
[17] Ottman G K, Hofmann H F, Bhatt A C and Lesieutre G A 2002 Adaptive piezoelectric energy harvesting circuit for wireless remote power supply *IEEE Trans. Power Electron.* **17** 669–76
[18] Liang J R and Liao W H 2008 Piezoelectric energy harvesting and dissipation on structural damping *J. Intell. Mater. Syst. Struct.* **20** 515–27
[19] Guyomar D, Badel A, Lefeuvre E and Richard C 2005 Toward energy harvesting using active materials and conversion improvement by nonlinear processing *IEEE Trans. Ultrason. Ferroelectr. Freq. Control* **52** 584–95
[20] Lallart M, Lefeuvre É, Richard C and Guyomar D 2008 Self-powered circuit for broadband, multimodal piezoelectric vibration control *Sens. Actuators* A **143** 377–82
[21] Richard C, Lefeuvre E and Guyomar D 2007 *Self-Powered Electronic Breaker With Automatic Switching by Detecting Maxima or Minima of Potential Difference Between its Power Electrodes* WO/2007/063194
[22] Liang J and Liao W H 2012 Improved design and analysis of self-powered synchronized switch interface circuit for piezoelectric energy harvesting systems *IEEE Trans. Ind. Electron.* **59** 1950–60
[23] Lefeuvre E, Badel A, Richard C, Petit L and Guyomar D 2006 A comparison between several vibration-powered piezoelectric generators for standalone systems *Sens. Actuators* A **126** 405–16

[24] Shu Y, Lien I and Wu W 2007 An improved analysis of the SSHI interface in piezoelectric energy harvesting *Smart Mater. Struct.* **16** 2253
[25] Lien I, Shu Y, Wu W, Shiu S and Lin H 2010 Revisit of series-SSHI with comparisons to other interfacing circuits in piezoelectric energy harvesting *Smart Mater. Struct.* **19** 125009
[26] Lien I and Shu Y 2012 Array of piezoelectric energy harvesting by the equivalent impedance approach *Smart Mater. Struct.* **21** 082001
[27] Lin H C, Wu P H, Lien I C and Shu Y C 2013 Analysis of an array of piezoelectric energy harvesters connected in series *Smart Mater. Struct.* **22** 094026
[28] Junrui L and Wei-Hsin L 2010 Impedance matching for improving piezoelectric energy harvesting systems *Proc. SPIE* **7643** 76430K
[29] Liang J and Liao W H 2012 Impedance modeling and analysis for piezoelectric energy harvesting systems *IEEE/ASME Trans. Mechatronics* **17** 1145–57
[30] Eltamaly A M and Addoweesh K E 2017 A novel self-power SSHI circuit for piezoelectric energy harvester *IEEE Trans. Power Electron.* **32** 7663–73
[31] Liang J and Liao W-H 2011 Energy flow in piezoelectric energy harvesting systems *Smart Mater. Struct.* **20** 015005
[32] Liang J R and Liao W H 2011 On the influence of transducer internal loss in piezoelectric energy harvesting with SSHI interface *J. Intell. Mater. Syst. Struct.* **22** 503–12
[33] Erturk A and Inman D J 2008 Issues in mathematical modeling of piezoelectric energy harvesters *Smart Mater. Struct.* **17** 065016
[34] Bayik B, Aghakhani A, Basdogan I and Erturk A 2016 Equivalent circuit modeling of a piezo-patch energy harvester on a thin plate with AC–DC conversion *Smart Mater. Struct.* **25** 055015
[35] Aghakhani A and Basdogan I 2017 Equivalent impedance electroelastic modeling of multiple piezo-patch energy harvesters on a thin plate with AC–DC conversion *IEEE/ASME Trans. Mechatronics* **22** 1575–84
[36] Chen Z, Xia Y, He J, Xiong Y and Wang G 2020 Elastic-electro-mechanical modeling and analysis of piezoelectric metamaterial plate with a self-powered synchronized charge extraction circuit for vibration energy harvesting *Mech. Syst. Signal Process.* **143** 106824
[37] Aghakhani A and Basdogan I 2018 Multiple piezo-patch energy harvesters on a thin plate with respective AC-DC conversion *Proc. SPIE* **10595** 105951B
[38] Cai Y, Zhang K, Ye Z, Liu C, Lu K and Wang L 2021 Influence of temperature on the natural vibration characteristics of simply supported reinforced concrete beam *Sensors* **21** 4242
[39] Lallart M, Wu Y-C and Guyomar D 2011 Switching delay effects on nonlinear piezoelectric energy harvesting techniques *IEEE Trans. Ind. Electron.* **59** 464–72